Int. J. Heat Mass Transfer. Vol. 23, pp. 161–177.

0017–9310/80/0201–0161 $02.00/0

FORCED FLOW LAMINAR FILMWISE CONDENSATION OF A PURE SATURATED VAPOR IN A VERTICAL TUBE

FLAVIO DOBRAN and RICHARD S. THORSEN

Department of Mechanical and Aerospace Engineering,
Polytechnic Institute of New York, Brooklyn, NY 11201, U.S.A.

(*Received* 3 *November* 1978 *and in revised form* 26 *April* 1979)

Abstract – An analytical study of steady laminar, filmwise condensation of a saturated vapor in forced flow in a vertical tube has been conducted for the case when the vapor velocity profile at the tube inlet is fully developed and the tube wall temperature is maintained constant.

Equations and boundary conditions governing the condensation process have been examined in detail in order to determine relevant parameters of the problem. For a wide range of conditions of practical interest it is found that the condensation process is governed by five parameters. These are the ratio of vapor Froude to Reynolds number, Buoyancy number, vapor to liquid viscosity ratio, liquid Prandtl number and Subcooling number.

A numerical solution of the resulting set of equations shows considerable differences in hydrodynamics and heat transfer with variations in these parameters. Comparison of the results with Nusselt's analytic solution of constant interphase shear is also made and it is found that at high pressures, high Prandtl numbers and high ratios of Froude to Reynolds numbers, his analytic solution underpredicts the condensation length and film thickness and overpredicts the interphase mass and heat transfer. Significant disparities at low Prandtl numbers are found between analytic and numerical solutions for heat-transfer results as well as the hydrodynamic results. These disparities are a consequence of neglecting inertia terms in the liquid and vapor equations of motion in the analytic model and their inclusion in the model presented in this work.

NOMENCLATURE

B_0, buoyancy number, $1 - \rho_g/\rho_l$;
Cp, specific heat at constant pressure;
D, $4\dfrac{Fr_0(1 - B_0)}{Re_0\mu^*}\Big/(2Fr_0Pr_l)$;
E, Eckert number, $U_0^2/[Cp_l(T_{sat} - T_w)]$;
$E_1, \ldots, E_{21}$, functions defined in [14];
$\mathbf{f}$, vector defined by equation (55);
F, function defined in [14];
Fr_0, Froude number, $U_0^2/(2r_0g)$;
g, gravitational constant;
G, function defined in [14];
Ga, Galilei number, gL^3/γ_l^2;
h, heat-transfer coefficient;
h_{lg}, enthalpy of evaporation;
I_1, I_2, functions defined in [14];
k, thermal conductivity;
L, condensation length;
L^*, non-dimensional condensation length, $L\gamma_l/(Pr_lr_0^2U_0)$;
$\dot{m}$, total mass flow-rate in the tube;
$\dot{m}_l$, liquid mass flow-rate;
$\dot{m}_l^*$, non-dimensional liquid mass flow-rate, $\dot{m}_l/\dot{m}$;
Nu, local Nusselt number, $2r_0h/k_l$;
$\overline{Nu}$, average Nusselt number, $\dfrac{1}{z^*}\displaystyle\int_0^{z^*} Nu\,dz^*$;
p, P, static pressure;
p^*, non-dimensional static pressure, $(p - p_0)/(\rho_1U_0^2)$;
Pr_l, Prandtl number, μ_lCp_l/k_l;
$\mathbf{q}$, heat flux vector;
r, radial coordinate;
r^*, non-dimensional radial coordinate, r/r_0;
r_0, inner tube radius;
Re_0, Reynolds number of vapor at the tube inlet, $\rho_gU_02r_0/\mu_g$;
S_0, subcooling number, $Cp_l(T_{sat} - T_w)/h_{lg}$;
T, temperature;
u, axial velocity;
u^*, non-dimensional axial velocity, u/U_0;
U_0, average flow velocity of vapor entering the tube;
v, radial velocity;
v^*, non-dimensional radial velocity, $Pr_l\dfrac{vr_0}{\gamma_l}$;
$\mathbf{V}$, velocity vector;
$\mathbf{y}$, vector $(y_1, y_2, y_3)^T$;
y_1, non-dimensional liquid film thickness, η;
y_2, non-dimensional derivative of the condensate flow-rate, $d\dot{m}_l^*/dz^*$;
y_3, non-dimensional derivative of the condensate flow-rate, $d\dot{m}_l^*/dz^*$;
z, axial coordinate;
z^*, non-dimensional axial coordinate, $z\gamma_l/(Pr_lr_0^2U_0)$.

Greek symbols

Δ, thickness of the vapor core;
Δ_z, $d\Delta/dz$;
η, non-dimensional vapor core thickness, Δ/r_0;
η_{z^*}, $d\eta/dz^*$;

θ, non-dimensional temperature ratio, $(T - T_w)/(T_{sat} - T_w)$;
μ, dynamic voscosity;
μ^*, viscosity ratio, μ_g/μ_l;
γ, kinematic viscosity;
ρ, mass density;
τ, stress tensor;
τ_{ij}, shear stress acting on the surface i and in the direction j;
ϕ, angle in Fig. 1;
Φ, dissipation function.

Subscripts

f, film;
g, vapor;
l, liquid;
0, at the tube inlet;
R, reference;
sat, saturation state;
w, wall of the tube.

Superscripts

g, vapor;
l, liquid;
T, transpose.

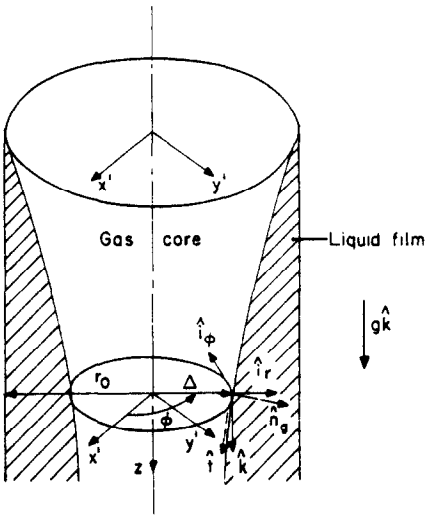

FIG. 1. Filmwise condensation in a vertical tube.

INTRODUCTION

THE CONDENSATION of pure vapors in vertical tubes has been studied extensively [1–10]. These experimental and analytical studies have been concerned primarily with wetting fluids which condense filmwise and with the tube surface kept at a uniform temperature. The vapor temperature at the tube inlet is considered to be saturated or superheated and the vapor velocity profile as either fully developed or uniform.

The complexity of thermo-hydrodynamic coupling of the liquid and vapor phases has resulted in a myriad of correlations which attempt to present heat-transfer and pressure drop results in various regimes of the tube condensation process. For most part these correlations have the liquid–vapor interphase shear stress determined from the adiabatic co-current liquid–vapor flow results. This is evident in the analyses of Carpenter and Colburn [3], Dukler [4] and others. No analytic treatment exists which is free from a semi-empirical approach and which is consistent with the process of condensation in the vertical tube. This applies equally well to all regimes of flow.

It is the purpose of this paper to critically examine the governing equations describing the filmwise condensation in a vertical tube under laminar liquid–vapor flow, to determine a set of parameters describing this condensation process and to present an approximate solution to a consistent set of equations in terms of these parameters for both hydrodynamics and heat transfer.

PROBLEM UNDER INVESTIGATION AND GOVERNING EQUATIONS

Steady, laminar, filmwise condensation of a pure vapor in a vertical tube with downflow is considered. The vapor entering the tube is saturated and its velocity profile is fully developed. Also, the tube surface temperature is taken to be constant. Figure 1 illustrates this condensation process schematically and defines the nomenclature in the cylindrical coordinate system for the problem.

The problem is formulated utilizing classical field theory [11] and the fluid is linear Stokesian. Furthermore, the following assumptions are made to simplify the formulation without compromising the essential features.

1. Liquid and vapor phases are incompressible.
2. Fluid properties are constant.
3. Absence of interfacial line fluxes (such as surface tension).
4. No interfacial resistance to heat transfer.
5. The vapor core is saturated.
6. Saturation temperature difference between any point in the vapor core and the inlet to the tube is much less than the difference in temperatures between vapor at the tube inlet and the tube surface.

Conservation equations for liquid and vapor phases

$$\frac{1}{r}\frac{\partial}{\partial r}(rv_m) + \frac{\partial u_m}{\partial z} = 0 \tag{1}$$

$$\rho_m\left(v_m\frac{\partial v_m}{\partial r} + u_m\frac{\partial v_m}{\partial z}\right) = -\frac{\partial p_m}{\partial r} + \frac{1}{r}\frac{\partial}{\partial r}(r\tau_{rr}^m) - \frac{\tau_{\phi\phi}^m}{r} + \frac{\partial \tau_{zr}^m}{\partial r} \tag{2}$$

$$\rho_m\left(v_m\frac{\partial u_m}{\partial r} + u_m\frac{\partial u_m}{\partial z}\right) = -\frac{\partial p_m}{\partial z} + \rho_m g + \frac{1}{r}\frac{\partial}{\partial r}(r\tau_{rz}^m) + \frac{\partial \tau_{zz}^m}{\partial z} \tag{3}$$

$$\rho_l C p_l \left(v_l \frac{\partial T_l}{\partial r} + u_l \frac{\partial T_l}{\partial z} \right) = \frac{1}{r} \frac{\partial}{\partial r} \left(r k_l \frac{\partial T_l}{\partial r} \right) + \frac{\partial}{\partial z} \left(k_l \frac{\partial T_l}{\partial z} \right) + \Phi^l \quad (4)$$

$$T_g = T_{sat}(p_g). \quad (5)$$

In equations (1)–(3) $m = l$ denotes the liquid phase and $m = g$ denotes the vapor phase.

Liquid–vapor interface equations

$$(\rho_l \mathbf{V}_l \sim \rho_g \mathbf{V}_g)_{r=\Delta} \cdot \hat{n}_g = 0 \quad (6)$$

$$[\rho_g \mathbf{V}_g (\mathbf{V}_g \cdot \hat{n}_g) - \tau_g \cdot \hat{n}_g]_{r=\Delta} - [\rho_l \mathbf{V}_l (\mathbf{V}_l \cdot \hat{n}_g) - \tau_l \cdot \hat{n}_g]_{r=\Delta} + (p_g - p_l)_{r=\Delta} \hat{n}_g = 0 \quad (7)$$

$$\left[\rho_g \mathbf{V}_g \left(h_{lg} + \frac{V_g^2 - V_l^2}{2} \right) - \mathbf{q}_l + \tau_l \cdot \mathbf{V}_l - \tau_g \cdot \mathbf{V}_g \right]_{r=\Delta} \cdot \hat{n}_g = 0 \quad (8)$$

No-slip conditions at the interface

Taking the scalar product of momentum equation (7) with the unit tangent vector at the interface and utilizing the interface conservation of mass equation (6) results in

$$\{(\rho_g \mathbf{V}_g \cdot \hat{n}_g)(\mathbf{V}_g \cdot \mathbf{t} - \mathbf{V}_l \cdot \mathbf{t}) - [(\tau_g \cdot \hat{n}_g) \cdot \hat{t} - (\tau_l \cdot \hat{n}_g) \cdot \hat{t}]\}_{r=\Delta} = 0. \quad (9)$$

This result shows that no-slip of tangential velocities at the interface implies no-slip of tangential shears and vice versa. These conditions are justified separately within the framework of classical field theory. Therefore

$$(\mathbf{V}_g - \mathbf{V}_l)_{r=\Delta} \cdot \hat{t} = 0$$

$$\text{or} \quad \left[u_g - u_l - (v_l - v_g) \frac{d\Delta}{dz} \right]_{r=\Delta} = 0 \quad (10)$$

and

$$[(\tau_g \cdot \hat{n}_g) - (\tau_l \cdot \hat{n}_g)]_{r=\Delta} \cdot \hat{t} = 0$$

or

$$[\tau_{zr}^l (1 - \Delta_z^2) + \Delta_z (\tau_{rr}^l - \tau_{zz}^l) - \tau_{zr}^g (1 - \Delta_z^2) - \Delta_z (\tau_{rr}^g - \tau_{zz}^g)]_{r=\Delta} = 0. \quad (11)$$

Constitutive equations

$$\left.\begin{aligned} &\tau_{rr}^m = 2\mu_m \frac{\partial v_m}{\partial r}, \quad \tau_{\phi\phi}^m = 2\mu_m \frac{v_m}{r}, \quad \tau_{zz}^m = 2\mu_m \frac{\partial u_m}{\partial z} \\ &\tau_{rz}^m = \tau_{zr}^m = \mu_m \left(\frac{\partial u_m}{\partial r} + \frac{\partial v_m}{\partial z} \right), \\ &\tau_{r\phi}^m = \tau_{\phi r}^m = \tau_{\phi z}^m = \tau_{z\phi}^m = 0 \\ &\mathbf{g}_l = -k_l \nabla T_l. \end{aligned}\right\} \quad (12)$$

Boundary conditions

$$u_g(z = 0, r) = 2u_0 \left(1 - \frac{r^2}{r_0^2} \right), \quad v_g(z = 0, r) = 0, \quad \frac{\partial u_g(z, r = 0)}{\partial r} = 0 \quad (13a, b, c)$$

$$v_g(z, r = 0) = 0, \quad u_g(z = L, r) = 0, \quad v_g(z = L, r) = 0 \quad (14a, b, c)$$

$$u_l(z = 0, r) = 0, \quad v_l(z = 0, r) = 0, \quad u_l(z, r = r_0) = 0 \quad (15a, b, c)$$

$$v_l(z, r = r_0) = 0, \quad \frac{\partial u_l}{\partial z}(z = L, r) = 0, \quad v_l(z = L, r) = 0 \quad (16a, b, c)$$

$$T_l(z, r = r_0) = T_w, \quad T_l(z, r = \Delta) = T_{sat}(\Delta) \quad (17a, b)$$

$$T_l(z = 0, r) = T_{sat}(r, z = 0), \quad \frac{\partial T_l(z = L, r)}{\partial z} = 0 \quad (18a, b)$$

$$p(z = 0, r) = p_0. \quad (19)$$

Parameters of the condensation process and non-dimensional equations

For purposes of determining a set of dimensionless parameters describing the present condensation problem, reference quantities for dependent and independent variables are introduced as follows.

$$r^* = \frac{r}{r_R}, \quad z^* = \frac{z}{z_R}, \quad u_l^* = \frac{u_l}{u_{lR}}, \quad v_l^* = \frac{v_l}{v_{lR}}$$

$$u_g^* = \frac{u_g}{u_{gR}}, \quad v_g^* = \frac{v_g}{v_{gR}}, \quad p_l^* = \frac{p_l - p_A}{p_{lR}}$$

$$p_g^* = \frac{p_g - p_A}{p_{gR}}, \quad \theta_l = \frac{T_l - T_A}{T_R}, \quad \theta_g = \frac{T_g - T_A}{T_R}.$$

Substituting the new variables into equations (1)–(19) yields a non-dimensional set of equations with parameters expressed in terms of original parameters and the reference quantities. To determine expressions for the reference quantities these equations are first examined for the number of independent parameters expressable in terms of reference quantities and fluid properties. This procedure yields an overdetermined system where the number of parameters exceeds the number of reference quantities and consequently precludes the reduction in the number of independent variables describing the process. The determination of reference quantities, described in detail in [15], results in the following choices:

$$r_R = r_0, \quad z_R = Pr_l \frac{r_0^2 U_0}{\gamma_l}, \quad u_{lR} = u_{gR} = U_0,$$

$$v_{lR} = v_{gR} = \frac{\gamma_l}{Pr_l r_0}, \quad p_{lR} = p_{gR} = \rho_l U_0^2, \quad p_A = p_0,$$

$$T_A = T_w, \quad T_R = T_{sat}(0) - T_w.$$

It is noted that the appearance of dynamic pressure as the reference pressure is consistent with the incompressible flow assumption.

In dimensionless form the governing equations are described by seven independent parameters. These are the liquid Prandtl number Pr_l, subcooling number S_0, buoyancy number B_0, vapor to liquid viscosity ratio μ^*, Eckert number E, ratio of Froude to Reynolds number Fr_0/Re_0 and the parameter

$$4\frac{Fr_0}{Re_0}\frac{(1-B_0)}{\mu^*}\Big/(2Fr_0Pr_l).$$

These equations are presented below.

Note that in these equations

if $m = l$ (liquid) then $n = 1$ and $j = 1$

if $m = g$ (vapor) then $n = 1 - B_0$ and $j = \mu^*$.

A. Field equations

$$\frac{1}{r^*}\frac{\partial}{\partial r^*}(r^* v_m^*) + \frac{\partial u_m^*}{\partial z^*} = 0 \tag{20}$$

$$nD^2\left\{v_m^*\frac{\partial v_m^*}{\partial r^*} + u_m^*\frac{\partial v_m^*}{\partial z^*}\right\} = -\frac{\partial p_m^*}{\partial r^*} + \frac{1}{r^*}\frac{\partial}{\partial r^*}(r^*\tau_{r^*r^*}^{*m}) - \frac{\tau_{\phi\phi}^{*m}}{r^*} + D\frac{\partial \tau_{z^*r^*}^{*m}}{\partial z^*} \tag{21}$$

$$n\left\{v_m^*\frac{\partial u_m^*}{\partial r^*} + u_m^*\frac{\partial u_m^*}{\partial z^*}\right\} = -\frac{\partial p_m^*}{\partial z^*} + \frac{nPr_l}{4Fr_0(1-B_0)/Re_0\mu^*} + \frac{1}{D}\frac{1}{r^*}\frac{\partial}{\partial r^*}(r^*\tau_{r^*z^*}^{*m}) + \frac{\partial \tau_{z^*z^*}^{*m}}{\partial z^*} \tag{22}$$

$$v_l^*\frac{\partial \theta_l}{\partial r^*} + u_l^*\frac{\partial \theta_l}{\partial z^*} = \frac{1}{r^*}\frac{\partial}{\partial r^*}\left(r^*\frac{\partial \theta_l}{\partial r^*}\right) + D^2\frac{\partial^2\theta_l}{\partial z^{*2}} + EPr_l\Phi^{*l} \tag{23}$$

$$\theta_g = 1. \tag{24}$$

B. Interface and constitutive equations

Conservation of mass at the interface

$$\{(1-B_0)(v_g^* - u_g^*\eta_{z^*}) - (v_l^* - u_l^*\eta_{z^*})\}_{r^*=\eta} = 0. \tag{25}$$

Tangential velocity matching at the interface (no-slip condition)

$$\{u_g^* - u_l^* - D^2\eta_{z^*}(v_l^* - v_g^*)\}_{r^*=\eta} = 0. \tag{26}$$

Tangential component of the interface momentum equation

$$\{(1 - D^2\eta_{z^*}^2)[\tau_{z^*r^*}^{*l} - \tau_{z^*r^*}^{*g}] + D\eta_{z^*}[(\tau_{r^*r^*}^{*l} - \tau_{z^*z^*}^{*l}) - (\tau_{r^*r^*}^{*g} - \tau_{z^*z^*}^{*g})]\}_{r^*=\eta} = 0. \tag{27}$$

Normal component of the interface momentum equation

$$\{D^2(v_l^* - u_l^*\eta_{z^*})(v_g^* - v_l^*) + (p_g^* - p_l^*) - [\tau_{r^*r^*}^{*g} - \tau_{r^*r^*}^{*l} + \eta_{z^*}(\tau_{r^*z^*}^{*l} - \tau_{r^*z^*}^{*g})]\}_{r^*=\eta} = 0. \tag{28}$$

Conservation of energy at the interface

$$\left\{(v_l^* - u_l^*\eta_{z^*})\left(\frac{1}{S_0} + \frac{E}{2}[u_g^{*2} - u_l^{*2} + D^2(v_g^{*2} - v_l^{*2})]\right) + \left(\frac{\partial \theta_l}{\partial r^*} - D^2\eta_{z^*}\frac{\partial \theta_l}{\partial z^*}\right) + E\left[\left[v_l^*\tau_{r^*r^*}^{*l} + \frac{1}{D}u_l^*\tau_{r^*z^*}^{*l} - D\eta_{z^*}\left(v_l^*\tau_{z^*r^*}^{*l} + \frac{1}{D}u_l^*\tau_{z^*z^*}^{*l}\right) - \left(v_g^*\tau_{r^*r^*}^{*g} + \frac{1}{D}u_g^*\tau_{r^*z^*}^{*g}\right) + D\eta_{z^*}\left(v_g^*\tau_{z^*r^*}^{*g} + \frac{1}{D}u_g^*\tau_{z^*z^*}^{*g}\right)\right]\right]\right\}_{r^*=\eta} = 0. \tag{29}$$

Where

$$\tau_{r^*r^*}^{*m} = 2jD^2Pr_l\frac{\partial v_m^*}{\partial r^*}$$

$$\tau_{\phi\phi}^{*m} = 2jD^2Pr_l\frac{v_m^*}{r^*}$$

$$\tau_{z^*z^*}^{*m} = 2jD^2Pr_l\frac{\partial u_m^*}{\partial z^*}$$

$$\tau_{z^*r^*}^{*m} = \tau_{r^*z^*}^{*m} = jDPr_l\left(\frac{\partial u_m^*}{\partial r^*} + D^2\frac{\partial v_m^*}{\partial z^*}\right)$$

$$\tau_{r^*\phi}^{*m} = \tau_{\phi r^*}^{*m} = \tau_{\phi z^*}^{*m} = \tau_{z^*\phi}^{*m} = 0.$$

C. Boundary conditions

$$u_g^*(z^*=0, r^*) = 2(1-r^{*2}), \quad v_g^*(z^*=0, r^*) = 0, \quad \frac{\partial u_g^*(z^*, r^*=0)}{\partial r^*} = 0 \tag{30a, b, c}$$

$$v_g^*(z^*, r^*=0) = 0, \quad u_g^*(z^*=L^*, r^*) = 0, \quad v_g^*(z^*=L^*, r^*) = 0 \tag{31a, b, c}$$

$$u_l^*(z^*=0, r^*) = 0, \quad v_l^*(z^*=0, r^*) = 0, \quad u_l^*(z^*, r^*=1) = 0 \tag{32a, b, c}$$

$$v_l^*(z^*, r^*=1) = 0, \quad \frac{\partial u_l^*(z^*=L^*, r^*)}{\partial z^*} = 0, \quad v_l^*(z^*=L^*, r^*) = 0 \tag{33a, b, c}$$

$$\theta_l(z^*, r^*=1) = 0, \quad \theta_l(z^*, r^*=\eta) = 1 \tag{34, a, b}$$

$$\theta_l(z^*=0, r^*) = 1, \quad \frac{\partial \theta_l(z^*=L^*, r^*)}{\partial z^*} = 0 \tag{35, a, b}$$

$$p^*(z^*=0, r^*) = 0. \tag{36}$$

The seven parameters which appear in foregoing equations define an eliptic problem and the solution in full generality is prohibitive. These equations will now be simplified.

SIMPLIFIED SET OF GOVERNING EQUATIONS

The parameters which appear in equations (20)–(36) are first evaluated for operating pressure levels, saturation to wall temperature differences and the tube inlet vapor velocities which are representative of anticipated applications. Table 1 shows the range for a number of substances of interest.

It is observed that in the range of practical interest the Eckert number E is very small, signifying the relative unimportance of the viscous dissipation term in the energy equation (23) and kinetic energy and viscous workrate terms in the energy interface equation (29). Another parameter which is very small for wide range of conditions, except for liquid metals with low vapor velocities, is D. Neglecting terms containing this parameter is theoretically much less justified than neglecting terms which are multiplied by the Eckert number. The reason for this is that in the former case the elliptic equations are reduced to parabolic equations and in turn some boundary conditions are ignored; e.g. equations (31b, c), (33b, c) and (35b).

If the eliptic problem continuously depends on the parameter D then the solution of the parabolic problem, which is absent of D, will be the same as the corresponding solution to the eliptic problem in the limit as $D \to 0$. Assuming the validity of foregoing statement, a simplified set of equations can be written for small values of D. Small Eckert number approximation is also taken into consideration.

A. Field equations

$$\frac{1}{r^*}\frac{\partial}{\partial r^*}(r^* v_m^*) + \frac{\partial u_m^*}{\partial z^*} = 0 \tag{37}$$

$$\frac{\partial p_m^*}{\partial r^*} = 0 \tag{38}$$

$$n\left\{v_m^*\frac{\partial u_m^*}{\partial r^*} + u_m^*\frac{\partial p_m^*}{\partial z^*}\right\} = -\frac{\partial u_m^*}{\partial z^*} + \frac{hPr_l}{4Fr_0(1-B_0)} + \frac{jPr_l}{Re_0\mu^*}\frac{1}{r^*}\frac{\partial}{\partial r^*}\left(r^*\frac{\partial u_m^*}{\partial r^*}\right) \tag{39}$$

$$v_l^*\frac{\partial \theta_l}{\partial r^*} + u_l^*\frac{\partial \theta_l}{\partial z^*} = \frac{1}{r^*}\frac{\partial}{\partial r^*}\left(r^*\frac{\partial \theta_l}{\partial r^*}\right) \tag{40}$$

$$\theta_g = 1. \tag{41}$$

B. Interface equations

$$\{(1-B_0)(v_g^* - u_g^*\eta_{z^*}) - (v_l^* - u_l^*\eta_{z^*})\}_{r^*=\eta} = 0 \tag{42}$$

$$\{u_g^* - u_l^*\}_{r^*=\eta} = 0 \tag{43}$$

$$\left\{\frac{\partial u_l^*}{\partial r^*} - \mu^*\frac{\partial u_g^*}{\partial r^*}\right\}_{r^*=\eta} = 0 \tag{44}$$

$$\{p_g^* - p_l^*\}_{r^*=\eta} = 0 \tag{45}$$

$$\left\{(v_l^* - u_l^*\eta_{z^*}) + S_0\frac{\partial \theta_l}{\partial r^*}\right\}_{r^*=\eta} = 0 \tag{46}$$

C. Boundary conditions

$$u_g^*(z^*=0, r^*) = 2(1-r^{*2}), \quad v_g^*(z^*=0, r^*) = 0, \quad \frac{\partial u_g^*(z^*, r^*=0)}{\partial z^*} = 0 \tag{47a, b, c}$$

$$v_g^*(z^*, r^*=0) = 0, \quad u_l^*(z^*=0, r^*) = 0, \quad v_l^*(z^*=0, r^*) = 0 \tag{48a, b, c}$$

$$u_l^*(z^*, r^*=1) = 0, \quad v_l^*(z^*, r^*=1) = 0, \quad \theta_l(z^*, r^*=1) = 0 \tag{49a, b, c}$$

$$\theta_l(z^*, r^*=\eta) = 1, \quad \theta_l(z^*=0, r^*) = 1, \quad p^*(z^*=0, r^*) = 0. \tag{50a, b, c}$$

Equations (38) and (45) imply no radial variation in pressure and consequently, in the presentation to follow, this dependence will be omitted. The simplified set of equations also contain a number of the "usual" equations which are often utilized in the condensation heat transfer. These equations are (43), (44) and (46).

APPROXIMATE SOLUTION OF THE SIMPLIFIED EQUATIONS

Reduction to ordinary differential equations

Solution of the parabolic set of equations (37)–(50) is possible through a direct numerical parabolic scheme. However, in an attempt to further simplify the computational requirements an integral analysis with assumption of parabolic axial velocity profiles in the vapor and liquid, and a parabolic temperature profile in the liquid is introduced. This reduces the governing equation-set to a pair of ordinary differential equations.

The functional forms

$$u_l^* = a_1 + b_1 r^* + c_1 r^{*2}, \quad u_g^* = a_2 + b_2 r^* + c_2 r^{*2} \quad \text{and} \quad \theta_l = a_3 + b_3 r^* + c_3 r^{*2} \tag{51a, b, c}$$

are introduced for the liquid and vapor velocity profiles and liquid temperature profile. They contain nine variable coefficients which can be expressed in terms of boundary conditions and interface relations. Closure conditions for mass flow-rates of each phase are also introduced, i.e.

$$\dot{m}_l^* = \frac{2}{1-B_0}\int_\eta^1 r^* u_l^*\,dr^*, \quad \dot{m}_g^* = 2\int_0^\eta r^* u_g^*\,dr^* \tag{52.a, b}$$

Reduction of the partial differential equations leading to ordinary differential equations can only be outlined here. Details can be found in [15].

Using the continuity equations, equation (37), the axial momentum equation for the liquid is integrated across the liquid film and the vapor axial momentum equation is integrated across the vapor core. Radial integration is performed by utilizing the assumed form of velocity profiles and the pressure gradient is eliminated between these two equations. The result is a first order ordinary differential equation describing the liquid film thickness and condensate mass flow-rate.

Table 1. Range of parameters in typical applications

Substance	Pressure ($Pa \times 10^{-5}$)	T_{sat} (K)	Vapor velocity U_0 (m/s)	$T_{sat} - T_w$ (K)	Tube diameter D (m)	Re_0	$\frac{Fr_0}{Re_0}$	B_0	μ^*	Pr_l	S_0	E	$4\frac{Fr_0(1-B_0)}{Re_0\mu^*}$	$\left\{4\frac{Fr_0(1-B_0)}{Re_0\mu^*}\right\}^2 \Big/ 4Fr_0^2Pr_l^2$
Steam [11]	1.01	373	3	20	2×10^{-2}	2960	0.0152	0.9994	0.043	1.72	0.037	10^{-4}	8.8×10^{-4}	3.2×10^{-11}
	86	673	0.05	20	2×10^{-2}	2336	5.3×10^{-6}	0.935	0.22	0.96	0.082	2×10^{-8}	6.3×10^{-6}	6.9×10^{-8}
	1.01	373	0.01	20	2×10^{-2}	9.9	5.1×10^{-7}	0.9994	0.043	1.72	0.037	1.1×10^{-9}	2.9×10^{-6}	2.9×10^{-6}
Ammonia [11]	6.8	286	0.5	5	2×10^{-2}	5560	2.2×10^{-4}	0.9914	0.042	2.08	2×10^{-3}	10^{-4}	1.8×10^{-4}	1.2×10^{-9}
Freon 12 [11]	12.15	323	0.1	20	2×10^{-2}	9141	5.5×10^{-6}	0.944	9.1×10^{-2}	2.38	0.17	4.7×10^{-7}	1.4×10^{-5}	3.2×10^{-9}
Mercury [11]	2.1	673	1	20	2×10^{-2}	2287	2.2×10^{-3}	0.9994	7.7×10^{-2}	0.0104	9.3×10^{-3}	3.7×10^{-4}	6.8×10^{-5}	6.2×10^{-3}
Sodium [11]	1.504	1200	3	20	2×10^{-2}	852	5.3×10^{-2}	0.9995	1.8×10^{-4}	4.1×10^{-3}	6.7×10^{-3}	3.5×10^{-4}	0.621	2.83
	1.504	1200	10	20	2×10^{-2}	2840	0.176	0.9995	1.8×10^{-4}	4.1×10^{-3}	6.7×10^{-3}	3.9×10^{-3}	2.05	0.25
	1.504	1200	30	20	2×10^{-2}	8520	0.528	0.9995	1.8×10^{-4}	4.1×10^{-3}	6.7×10^{-3}	3.9×10^{-3}	6.21	0.028

$$\frac{d\eta}{dz^*}\left[\dot{m}_l^{*2}+\dot{m}_l^*\frac{5(3+\eta)(1-\eta^2)E_6E_{14}}{24\eta^3E_1E_{13}}+\frac{5\mu^*(1-\eta)^3(1+\eta)(3+10\eta+3\eta^2)I_1E_7E_{15}}{24(1-B_0)\eta^6E_1E_{13}}\right]+\frac{d\dot{m}_l^*}{dz^*}\left[\frac{(5+11\eta)(1-\eta)I_2E_5}{8E_1E_{13}}\times\left\{\dot{m}_l^*+\frac{5(1-\eta^2)(3+5\eta)E_{11}E_{16}}{6\eta^2(5+11\eta)I_2E_5}\right\}\right]$$

$$=\frac{Pr_l}{\left\{4\frac{Fr_0(1-B_0)}{Re_0\mu^*}\right\}}\times\left[\frac{5(3+5\eta)^2(1-\eta)^3(1+\eta)B_0E_7^2}{192(1-B_0)^2E_1E_{13}}+\frac{5(3+5\eta)}{2}\times\frac{Fr_0}{Re_0\mu^*}\frac{E_7E_8}{E_1E_{13}}\left\{\frac{\mu^*(1-\eta)^2(1+\eta)^2}{(1-B_0)\eta^4E_8}-\dot{m}_l^*\right\}\right]. \quad (53)$$

The non-dimensional functions (E's and I's) in the above equation depend on η, B_0 and μ^*, and are listed in [15].

Integrating the energy equation (40) across the liquid film and utilizing the assumed liquid velocity and temperature profiles results in a simplified governing heat transfer equation.

$$\frac{d^2\dot{m}_l^*}{dz^{*2}}+\frac{1}{\left\{\dot{m}_l^*E_{18}-\frac{2\mu^*(1-\eta)^2(1+\eta)}{3(1-B_0)\eta^2(3+4\eta)}\right\}}\times\left[\left[E_{18}\left(\frac{d\dot{m}_l^*}{dz^*}\right)^2+\frac{1}{4(1-B_0)}\left(\frac{d\dot{m}_l^*}{dz^*}\right)\times\frac{40(1+\eta)(3+5\eta)E_7}{(1-\eta)(3+4\eta)}\times\left\{1+S_0\frac{\eta(5+3\eta)E_{17}}{5(1+\eta)(3+5\eta)E_7}\right\}-\frac{S_0}{16(1-B_0)^2}\frac{640\eta(3+5\eta)E_7}{(1-\eta)^2(3+4\eta)}+\frac{d\eta}{dz^*}\left[\frac{d\dot{m}_l^*}{dz^*}\frac{2\mu^*(1-\eta)(6+15\eta+7\eta^2)}{3(1-B_0)\eta^3(3+4\eta)^2}\times\{1-\dot{m}_l^*E_{21}\}+\frac{S_0}{4(1-B_0)}\frac{\mu^*}{(1-B_0)}\times\frac{16(15+57\eta+49\eta^2+7\eta^3)}{3\eta^3(3+4\eta)(5+3\eta)}\{1-\dot{m}_l^*E_{20}\}+\frac{8S_0}{4(1-B_0)}\frac{(15+18\eta+23\eta^2)}{(1-\eta)^2(3+4\eta)^2}\times\left\{\dot{m}_l^*E_{17}-\frac{2\mu^*(1-\eta)^2(1+5\eta+2\eta)^2}{3(1-B_0)\eta^3(5+3\eta)}\right\}\times\left\{1-\frac{(5+3\eta)(9+30\eta+17\eta^2)E_{19}}{(3+5\eta)(15+18\eta+23\eta^2)}\right\}\right]-\frac{d\dot{m}_l^*}{dz^*}\frac{(9+30\eta+17\eta^2)E_{19}}{\eta(1-\eta)(3+4\eta)(3+5\eta)}\times\left\{\dot{m}_l^*E_{18}-\frac{2\mu^*(1-\eta)^2(1+\eta)}{3(1-B_0)\eta^2(3+4\eta)}\right\}\right]\Bigg]=0. \quad (54)$$

It is convenient to rewrite the foregoing equations as a system of *first order* differential equations. By letting $y_1=\eta$, $y_2=\dot{m}_l^*$ and $y_3=d\dot{m}_l^*/dz^*$ it follows that

$$\frac{dy_1}{dz^*}=F(y_1,y_2,y_3),\quad \frac{dy_2}{dz^*}=y_3,\quad \frac{dy_3}{dz^*}=G(y_1,y_2,y_3) \quad (55a)$$

where functions F and G are listed in [15]. This equation-set can also be written in a compact vector form as

$$\frac{d\mathbf{y}}{dz^*}=\mathbf{f}(\mathbf{y}). \quad (55b)$$

Solution of equations (55) requires initial conditions which can be set at $z^*=0$ where $y_1=1$ and $y_2=0$. As to the value of y_3 at $z^*=0$ it is not clear nor necessary to know for even if it is bounded the conditions for the existence and uniqueness of a solution to the set (55) are violated at this point. This violation is, perhaps, not surprising for discontinuity in tube wall temperature has been built into the model as well as parabolic form of equations utilized in the description of the condensation process.

For $0<z_0^*\le z^*\le a$ and prescribed initial value vector $\mathbf{y}(z_0^*)$, $\mathbf{f}$ is continuous with continuous first partial derivatives (see [15]). This, then, fulfils the conditions for the existence and uniqueness theorem [13] of ordinary differential equations and theorem [13] on the continuous dependence on the initial data. The problem is thus "well-posed" and perhaps amenable to the numerical computation.

The conclusion on the well-posedness of the initial value problem (55) away from $z^*=0$ rests upon the premise that initial values at $z_0^*>0$ can be specified. This is unfortunate for a solution in $z_0^*=0$ neighborhood is required to start the numerical computation and which is consistent with the boundary conditions of the present problem.

In 1916 Nusselt [1] obtained a closed form solution of the condensation process on a vertical surface by essentially ignoring thermohydrodynamic aspects of the vapor flow, liquid film inertia and liquid film convection. This solution has been slightly revised for usefulness in the present context and is reproduced in [15] and described by equations (56). The additional assumptions introduced by Nusselt should not be critical in the region z_0^* close to zero for here the liquid film is very thin and with negligible mass flow. As the boundary conditions and structure of highest order terms in equations of Nusselt are identical to the ones in present investigation it is possible to postulate that y_1, y_2 and y_3 from the two theories will overlap as $z^*\rightarrow$

0. This overlap is not necessary and "small" disagreement will not produce a meaningless solution of equations (55) as assured by their well-posedness.

To summarize, the solution of the governing equations (55) will be attempted under initial conditions

$$y_1(z_0^*) \text{ solved from } z_0^* = \frac{4\mu^*}{3S_0}[1 - y_1]^3 + \left[1 + \frac{32(1 - B_0)Fr_0}{B_0 Re_0}\right] \frac{B_0}{4S_0 \left\{\dfrac{4Fr_0(1 - B_0)}{Re_0 \mu^*}\right\}} \times [1 - y_1]^4 \quad (56a)$$

$$y_2(z_0^*) = \frac{4\mu^*}{(1 - B_0)}[1 - y_1(z_0^*)]^2 \times \left[\left[1 + \left[1 + \frac{32(1 - B_0)Fr_0}{B_0 Re_0}\right] \times \frac{Re_0 B_0}{Fr_0(1 - B_0)24}[1 - y_1(z_0^*)]\right]\right] \quad (56b)$$

$$y_3(z_0^*) = \frac{2S_0}{(1 - B_0)} \frac{1}{[1 - y_1(z_0^*)]} \quad (56c)$$

and with z_0^* "sufficiently small". The suitable choice of z_0^* is discussed below where we discuss the numerical method of solving equations (55).

Structure of the system of governing equations

Closed form solution of the system of equations (55) and initial conditions (56) is not possible and recourse to numerical computation is necessary. However, before any initial value numerical technique can be selected it is necessary that the structure of equations this technique is to solve be known. For this purpose a detailed study of the structure of governing equations was undertaken. This study involved the computation of local Jacobian matrix

$$\frac{\partial \mathbf{f}}{\partial \mathbf{y}} = \begin{pmatrix} \dfrac{\partial F}{\partial y_1} & \dfrac{\partial F}{\partial y_2} & \dfrac{\partial F}{\partial y_3} \\ 0 & 0 & 1 \\ \dfrac{\partial G}{\partial y_1} & \dfrac{\partial G}{\partial y_2} & \dfrac{\partial G}{\partial y_3} \end{pmatrix}$$

for different values of initial vectors. From this the local system response is determined from the characteristic equations. These computations point out that the governing equations (55) describe a process with time constants which diverge from each other as the liquid film thickness approaches zero. The spread in these time constants or the eigenvalues of the Jacobian matrix brings about severe computational requirements which can only be handled by stiff numerical methods.

Numerical procedure

The numerical procedure chosen to solve the system of equations (55) is described in [14]. It is a convergent procedure which can solve the stiff equations with relative ease. However, the improvements [15] built into the computational package have provided a reduction in computational time up to an order of 100.

For a wide range of the five arbitrary parameters the numerical procedure performed without difficulty. In all computations the initial vector is chosen according to equations (56) with an initial $\eta = 0.9996$.

Results

Numerical computation for y_1, y_2 and y_3 is carried out by specification of five parameters of the problem until all the vapor has condensed. It is recalled that these parameters are Fr_0/Re_0, B_0, μ^*, Pr_l and S_0. Once η, $\dot{m}_l^*$ and $d\dot{m}_l^*/dz^*$ (or y_1, y_2 and y_3) are determined numerically all other information follows readily and is described in [15]. Only the results will be presented here.

High Prandtl number plots of film thickness, condensate mass flow and derivative of condensate mass flow (interphase mass transfer) are shown in Figs. 2–4, respectively. In these figures all variables plotted are normalized to values at L^*, where L^* is the nondimensional length of tube where all the vapor has condensed. It is obtainable from the numerical solution. Also shown for comparison in the figures are values of variables obtained from analytic solution described by equations (56). Liquid film thickness, mass flow-rate, and its derivative at L^* are listed in Table 2 from both numerical and analytic solutions.

From Table 2 it is first observed that the analytic solution underestimates both the condensation length L^* and film thickness $1 - \eta(L^*)$. This effect is more pronounced at higher values of Fr_0/Re_0 and higher pressures (low B_0). For case 6 in the table L^* is underpredicted by 15% and $1 - \eta$ by 10%. $d\dot{m}_l^*/dz^*$ is overpredicted by 24%. Local behavior of results is also similar and can be traced to an assumption in the analytic solution where the interphase shear is assumed to be constant. In the numerical solution interphase shear is decreasing along the tube length.

Two limiting curves are also plotted in Figs. 2–4. These are cases corresponding to forced convection limit and body force limit in the analytic solution. Determination of L^*, $1 - \eta(L^*)$ and $d\dot{m}_l^*(L^*)/dz^*$ from equations (56) is accomplished by setting $\dot{m}_l^*(L^*) = 1$ in (56b) and solving for only one real root of $1 - \eta$ in this equation. This is then substituted into (56a) and (56c) to yield the remaining results.

Cases corresponding to low liquid Prandtl numbers are also listed in Table 2 and some of the results presented in Fig. 5. The difference between numerical and analytical solutions is significant and by no means unexpected. This is so since the analytic solution is independent of Prandtl number. The Prandtl number dependence enters in the present model through the inertia terms in the equations of motion which, in the case of analytic solution, is not considered. Drawing conclusions from low Prandtl number plots should procede with caution since the simple form of govern-

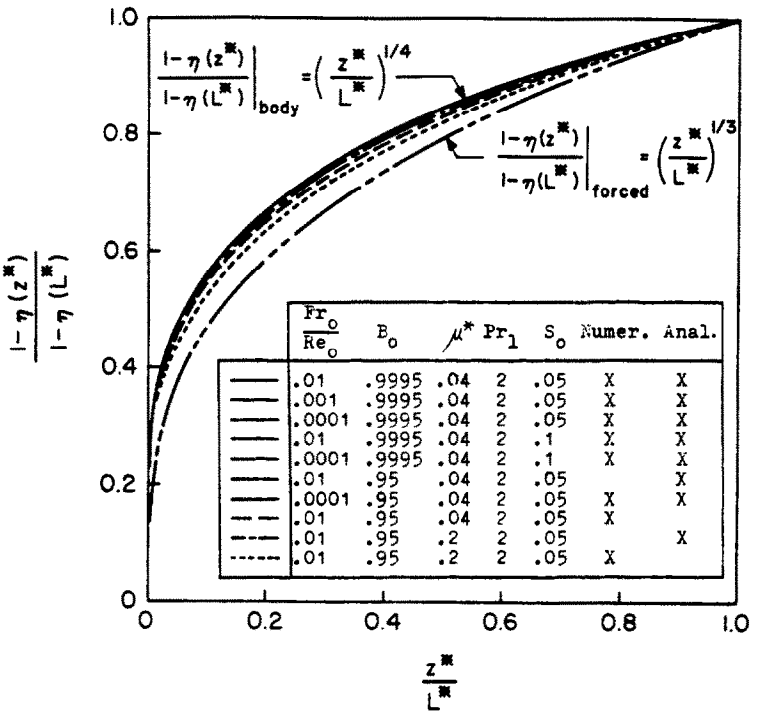

FIG. 2. Liquid film thickness distribution at $Pr_l = 2$.

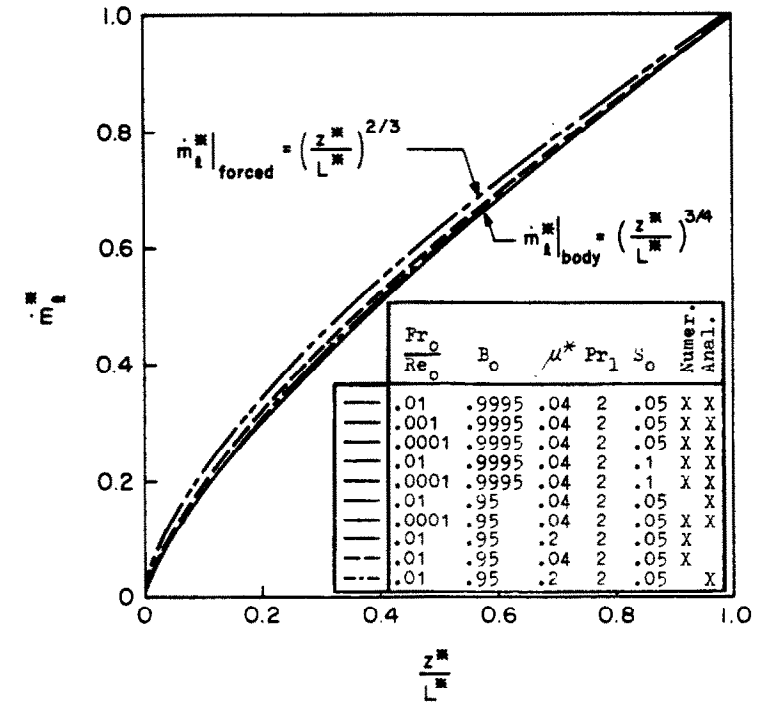

FIG. 3. Condensate mass flow-rate distribution at $Pr_l = 2$.

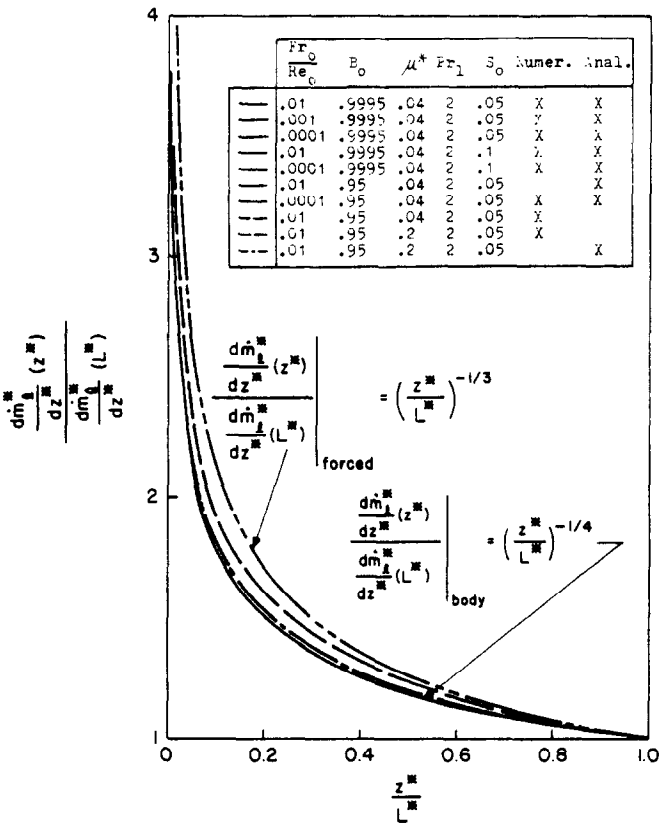

FIG. 4. Interphase mass-transfer distribution at $Pr_l = 2$.

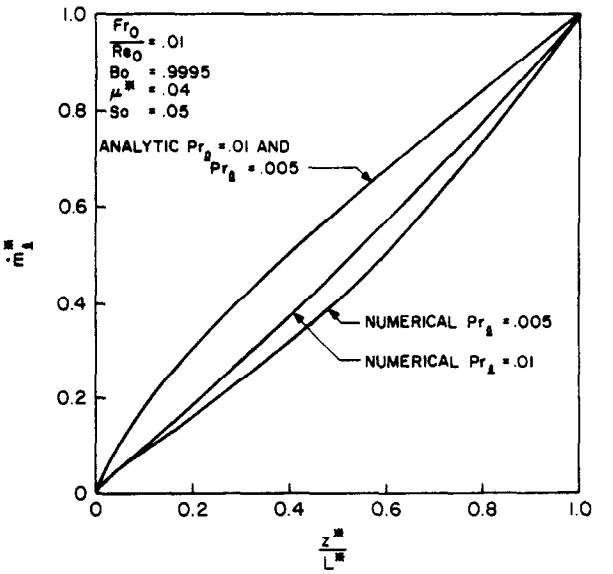

FIG. 5. Condensate mass flow-rate distribution at low Pr_l.

Table 2. Range of parameters involved in the parametric study and the associated values of condensation length; film thickness, interphase mass transfer, local and average Nusselt numbers at L^*

Case No.	$\frac{Fr_0}{Re_0}$	B_0	μ^*	Pr_l	S_0	L^* Numerical / L^* Analytic	$1-\eta(L^*)$ Numerical / $1-\eta(L^*)$ Analytic	$d\dot{m}_l^*/dz^*(L^*)$ Numerical / $d\dot{m}_l^*/dz^*(L^*)$ Analytic	$Nu(L^*)$ Numerical / $Nu(L^*)$ Analytic	$\overline{Nu}(L^*)$ Numerical / $\overline{Nu}(L^*)$ Analytic
1	0.01	0.9995	0.04	2.0	0.05	0.27435×10^{-4} 0.26852×10^{-4}	0.0072435 0.0071730	0.27254×10^{5} 0.27884×10^{5}	0.2777×10^{3} 0.2788×10^{3}	371.60 372.41
3	0.0001	0.9995	0.04	2.0	0.05	0.58784×10^{-5} 0.58266×10^{-5}	0.0015570 0.0015540	0.12716×10^{6} 0.12873×10^{6}	0.1295×10^{4} 0.1287×10^{4}	1725.20 1716.27
4	0.01	0.9995	0.04	2.0	0.1	0.13891×10^{-4} 0.13426×10^{-4}	0.0072520 0.007173	0.53946×10^{5} 0.55768×10^{5}	0.2798×10^{3} 0.2788×10^{3}	373.63 372.41
6	0.01	0.95	0.04	2.0	0.05	0.67336×10^{-1} 0.56949×10^{-1}	0.170263 0.153133	0.10546×10^{2} 0.13060×10^{2}	0.10780×10^{2} 0.13060×10^{2}	15.16 17.56
7	0.0001	0.95	0.04	2.0	0.05	0.13230×10^{-1} 0.12748×10^{-1}	0.034572 0.034006	0.56306×10^{2} 0.58813×10^{2}	0.57377×10^{2} 0.58810×10^{2}	77.02 78.44
8	0.01	0.95	0.2	2.0	0.05	0.36952×10^{-1} 0.32531×10^{-1}	0.098074 0.087952	0.19158×10^{2} 0.22739×10^{2}	0.19549×10^{2} 0.22740×10^{2}	27.605 30.74
10	0.01	0.9995	0.04	0.005	0.05	0.91867×10^{-4} 0.26852×10^{-4}	0.012723 0.007173	0.15478×10^{5} 0.27883×10^{5}	0.1577×10^{3} 0.2788×10^{3}	108.08 372.41
12	0.01	0.9995	0.04	2.0	0.005	0.27126×10^{-3} 0.26852×10^{-3}	0.007235 0.007173	0.27515×10^{4} 0.27884×10^{4}	0.27568×10^{3} 0.2788×10^{3}	369.42 372.41
15	0.01	0.9995	0.04	0.005	0.005	0.31476×10^{-3} 0.26852×10^{-3}	0.007681 0.007173	0.25910×10^{4} 0.27884×10^{4}	0.25961×10^{3} 0.27882×10^{3}	318.86 372.41
19	0.01	0.95	0.04	0.005	0.001	0.36692×10^{1} 0.28475×10^{1}	0.168738 0.153133	0.21517×10^{0} 0.26121×10^{0}	0.10764×10^{2} 0.13061×10^{2}	13.76 17.56
20	0.01	0.95	0.04	0.005	0.005	0.17203×10^{1} 0.56949×10^{0}	0.186919 0.153133	0.95969×10^{0} 0.13061×10^{1}	0.96049×10^{1} 0.13061×10^{2}	5.83 17.56

ing equations are less valid at low Froude numbers.

Hydrodynamic results

Significant hydrodynamic results include the distribution of pressure gradient and pressure along the length of tube. It is more convenient, however, to plot the results as a function of local vapor quality rather than the distance along the tube. Figures 6–9 illustrate various hydrodynamic results plotted in this manner for wide range of arbitrary parameters.

From Figs. 6 and 7 it is seen that the acceleration effects are much more pronounced at low Prandtl numbers and tend to dominate the overall pressure gradient.

Total pressure gradient and pressure distribution is illustrated in Figs. 8 and 9, respectively, for high Prandtl numbers. Figure 9 is significant for it allows the hydrodynamic design of the condenser units for wide range of operating conditions.

Heat-transfer results

The values of local and average Nusselt numbers at L^* are given in Table 2. Figure 10 shows the distribution of average value of the Nusselt number vs the subcooling number. From this figure it is concluded that at high values of Prandtl numbers and over wide range in subcooling numbers of practical interest, the analytic solution overpredicts the heat transfer for both, high values of the ratio Fr_0/Re_0 and at high pressures (low B_0). The explanation lies in the thickness of liquid film which is thinner from the analytic solution for the same set of parameters. This in turn leads to better heat transfer.

At low Prandtl numbers the analytic solution becomes invalid and Nusselt number deteriorates considerably. This reduction is caused by the large thermal conductivity of low Prandtl number fluids and motion (inertia) of the film. At large subcoolings this deterioration is even worse.

Comparison with the experiment

Local hydrodynamic and heat-transfer experimental data consistent with boundary conditions of this work does not exist. The type of data which is presented in the literature is in the form of average value of heat-transfer coefficient over the entire tube condensing surface. Even in such form most data presented cannot be compared with this work for the reason that the parameters fall outside the range of Table 1. At high Pr_l, low vapor velocity (laminar flow) and low pressure experimental data on the average Nusselt number agrees well with the analytic solution as is demonstrated in [2, 7], and the numerical solution is in agreement with the analytic solution in this range of parameters.

It is of interest, however, to see that reasonable comparison with the experiment can be achieved at high Pr_l numbers even if vapor Reynolds number Re_0 is very high. This is illustrated in Table 3 where two references have been chosen for this purpose. Wall

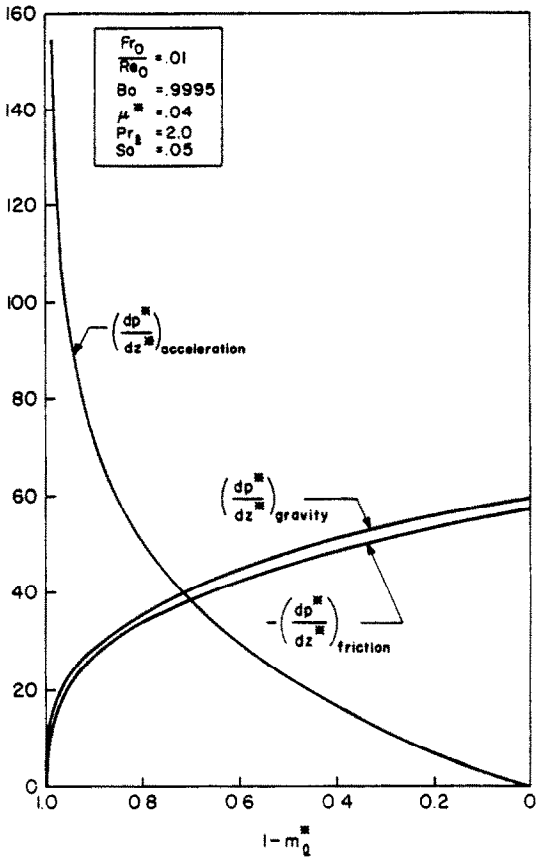

FIG. 6. Comparison of pressure gradients at high Fr_0/Re_0 and high Pr_l.

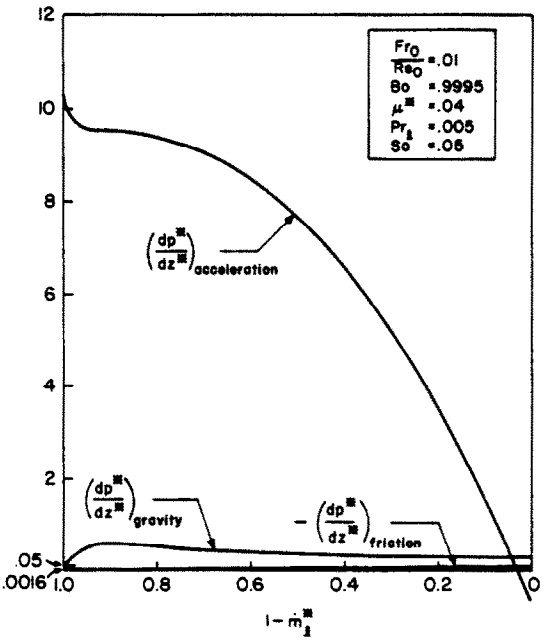

FIG. 7. Comparison of pressure gradients at low Pr_l.

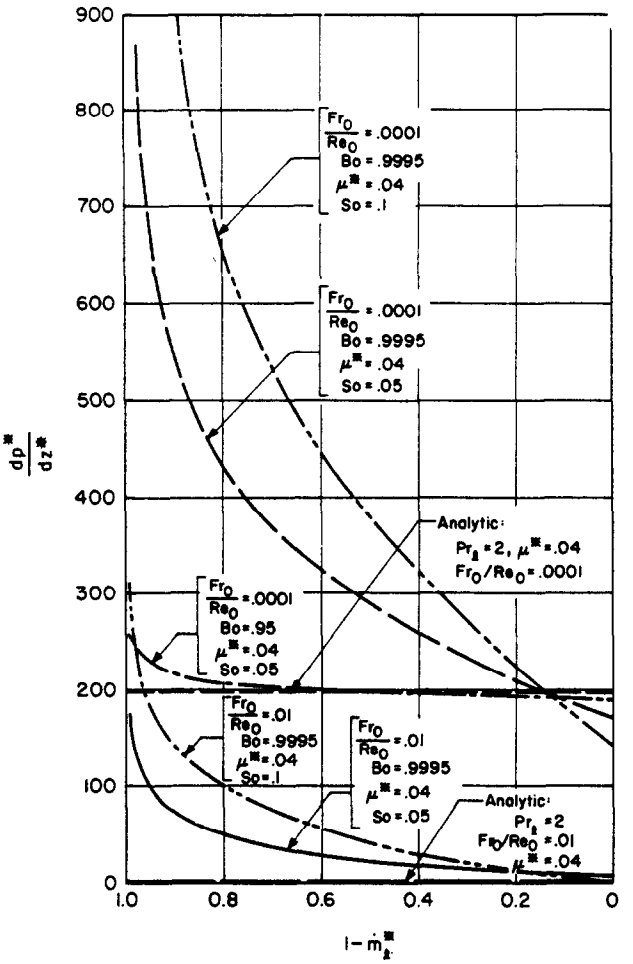

FIG. 8. Total pressure gradient distribution at $Pr_l = 2$.

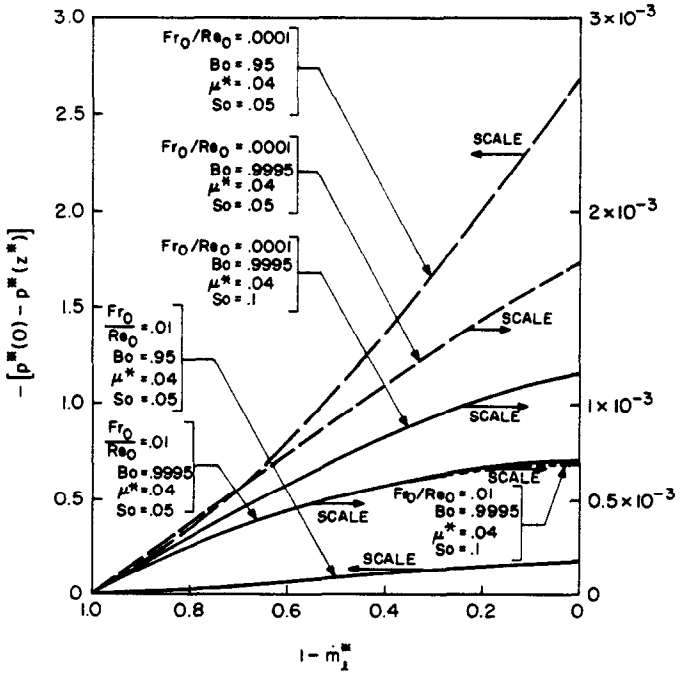

FIG. 9. Pressure distribution along the tube length of $Pr_l = 2$.

Table 3. Comparison of numerical and experimental data for the average Nusselt number at high values of Reynolds and Prandtl numbers

Ref. No.	Run in Ref.	Fluid	U_0 (m/s)	L (m)	D (m)	T_{sat} (K)	$T_{sat}-T_w$ (K)	$\overline{Nu}(L)$ exp.	Re_0	$\frac{Fr_0}{Re_0}$	B_0	μ^*	Pr_l	S_0	$\overline{Nu}(L)$ theory	$\frac{\overline{Nu}\text{/exp.} - \overline{Nu}\text{/theory}}{\overline{Nu}\text{/exp.}}$
2	Fig. 6	H_2O	20	1.21	0.04	373	28	325	39 500	0.0276	0.9994	0.035	2.31	0.0515	270	17%
2	Fig. 6	H_2O	40	1.21	0.04	373	28	475	79 000	0.0552	0.9994	0.035	2.31	0.0515	271	43%
2	Fig. 6	H_2O	20	1.21	0.04	373	11	369	36 900	0.0276	0.9994	0.0424	1.88	0.206	353.5	4%
2	Fig. 6	H_2O	40	1.21	0.04	373	11	491	73 800	0.0552	0.9994	0.0424	1.88	0.0206	358	27%
2	Fig. 6	H_2O	20	1.21	0.04	373	4	460	36 900	0.0276	0.9994	0.0424	1.88	0.00742	462	−0.4%
8	3	H_2O	48	2.35	0.0158	401	27	266	79 900	0.196	0.9986	0.0512	1.66	0.0518	128	52%
8	5	H_2O	20	2.32	0.0158	403	23.5	112	35 800	0.0744	0.9984	0.0547	1.56	0.0456	100	10%
8	13	H_2O	26.5	1.86	0.0158	400	29.5	154	44 600	0.10895	0.9986	0.0512	1.66	0.0572	90	41%

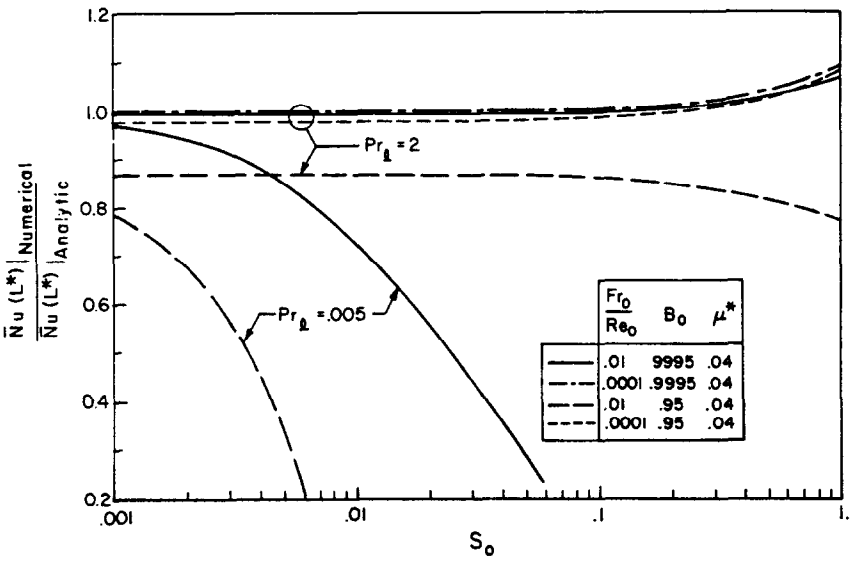

FIG. 10. The effect of various parameters on the average Nusselt number.

temperature of the tube in [8] is evaluated at $L/2$ while data from both references has been reduced by evaluating liquid properties at $T_f = T_w + 0.3(T_{sat} - T_w)$ and vapor properties at T_{sat}. From the table it can be seen that high values of Fr_0/Re_0 and S_0 lead to much higher values of Nusselt numbers than predicted by theory. At high values of parameter Fr_0/Re_0 and Prandtl numbers the induced turbulence in the film due to high vapor velocity is sufficient to dramatically increase the Nusselt number. High values of S_0 cause larger interphase mass-transfer rates which can lead to significant disturbance of the liquid–vapor interface for waves to start appearing. At high Pr_l increase in heat transfer is again possible due to such phenomena.

SUMMARY AND CONCLUSIONS

The main conclusions and summary of this work are as follows:

1. The defined tube condensation process is found to depend on a number of physical parameters. Low D and low E number approximation reduced the count to five. These are Fr_0/Re_0, B_0, μ^*, Pr_l and S_0.
2. Assumption of the form of velocity and temperature profiles reduced the coupled set of partial differential equations to three nonlinear and coupled ordinary differential equations.
3. The stiff set of ordinary differential equations is found to be well posed for initial conditions determined from the analytic solution of a simplified condensation process in the tube.
4. Numerical solution of the stiff set of equations has been carried out by an efficient and convergent computer code for wide range of arbitrary parameters.
5. Results from the numerical solution revealed no practical difference in heat transfer, condensate mass flow and film thickness between it and analytic solution of Nusselt for very low values of Fr_0/Re_0, high B_0 and high Pr_l. At high Fr_0/Re_0, low B_0 and high Pr_l disparities in results between analytic and numerical solutions can be significant.
6. Detailed hydrodynamic results for a wide range of parameters have been obtained for the first time in this study.
7. Significant results have also been obtained for low values of liquid Prandtl numbers. It is shown that the effect of inertia of vapor–liquid flow is in such circumstances significant.

REFERENCES

1. W. Nusselt, Die Oberflachenkondensation des Wasserdampfles, *Z. Ver. Dt. Ing.* **60**, 541, 546 (1916).
2. M. Jakob, Heat transfer in evaporation and condensation—II, *Mech. Engng* **58**, 729 (1936).
3. F. Carpenter and A. P. Colburn, The effect of vapor velocity on condensation inside tubes, in *Proceedings of a General Discussion of Heat Transfer*, M.E./A.S.M.E. (July 1951).
4. A. E. Dukler, Dynamics of vertical falling film systems, *Chem. Engng Prog.* **55**, (10), (1959).
5. H. R. Kunz and S. Yerazunis, An analysis of of film condensation, film evaporation and single-phase heat transfer for liquid Prandtl numbers from 10^{-3} to 10^{-4}, *J. Heat Transfer* **91**, (1969).
6. I. G. Shekriladze and S. A. Mestvirishvilli, Study of the process of film condensation of a flowing vapor within a vertical cylinder, *Heat Transfer—Soviet Res.* **4**(4), (1972).
7. V. P. Isachenko, F. Salomzoda and A. A. Shalakhov, An investigation of heat transfer with film condensation of steam in a vertical tube, *Teploenergetica* **21**, (1974).
8. J. H. Goodykoontz and R. G. Dorsch, Local heat transfer coefficients for condensation of steam in vertical downflow within a 5/8-inch diameter tube, NASA TN D-3326 (March 1966).
9. T. Ueda, T. Kubo and M. Inoue, Heat transfer for steam condensing inside a vertical tube, in *Proceedings of the Fifth International Heat Transfer Conference, Tokyo*, Vol. 3. A.S.M.E., New York (1975).

10. M. R. Berry and W. P. Goss, An integral analysis of condensing annular-mist flow, *A.I.Ch.E.Jl* **18**(4), (1972).
11. C. A. Eringen, *Continuum Physics*, Vol. 2. Academic Press, New York (1975).
12. N. B. Vargaftic, *Tables on the Thermophysical Properties of Liquids and Gases*, 2nd edn. Hemisphere, New York (1975).
13. H. Hochstadt, *Differential Equations*. Dover, New York (1975).
14. D. Lee, Numerical solutions of initial value problems, Naval Underwater Systems Center, NUSC Technical Report 5341 (1976).
15. F. Dobran, Forced flow laminar filmwise condensation of a pure saturated vapor in a vertical tube, Ph.D. Thesis, Polytechnic Institute of New York (1978).

CONDENSATION EN FILM LAMINAIRE D'UNE VAPEUR PURE SATUREE DANS UN TUBE VERTICAL

Résumé — On étudie analytiquement la condensation permanente en film laminaire d'une vapeur saturée en écoulement forcé dans un tube vertical, lorsque le profil de vitesse de la vapeur à l'entrée du tube est établi et la température pariétale est maintenue constante.

On examine en détail les équations et les conditions aux limites de façon à déterminer les paramètres caractéristiques du problème. Dans un large domaine de conditions d'intérêt pratique, on trouve que le mécanisme de condensation est gouverné par cinq paramètres : le rapport du nombre de Froude de la vapeur au nombre de Reynolds, le nombre d'Archimède, le rapport des viscosités de la vapeur et du liquide, le nombre de Prandtl du liquide et le nombre de sous-refroidissement.

Une solution numérique du système d'équations montre des différences considérables, sur l'hydrodynamique et sur le transfert thermique, en fonction de ces paramètres. Une comparaison des résultats avec la solution analytique de Nusselt montre qu'aux pressions élevées, aux forts nombres de Prandtl et aux grands rapports du nombre de Froude au nombre de Nusselt, la solution analytique sousestime le transfert massique à l'interface et le transfert thermique. Des différences significatives sont trouvées, aux faibles nombres de Prandtl, entre les solutions analytiques et numériques, pour les solutions hydrodynamiques et thermiques. Ces différences viennent de ce que les termes d'inertie sont négligés dans les équations du mouvement du liquide et de la vapeur dans le modèle analytique et ce travail présente leur prise en compte.

H.M.T.673

LAMINARE FILMKONDENSATION EINES REINEN GESÄTTIGTEN DAMPFES BEI ERZWUNGENER STRÖMUNG IN EINEM SENKRECHTEN ROHR

Zusammenfassung – In einem senkrechten Rohr wurde die stationäre laminare Filmkondensation von gesättigtem Dampf in erzwungener Strömung untersucht, und zwar für den Fall, daß der hydrodynamische Einlauf am Rohranfang abgeschlossen ist und die Rohrwandtemperatur konstant angenommen wird. Die Gleichungen und Randbedingungen, die den Kondensationsprozeß beschreiben, wurden im einzelnen untersucht, um die wesentlichen Parameter des Problems zu bestimmen. Für einen breiten Bereich von praktischen Anwendungsfällen wurde gefunden, daß der Kondensationsprozeß mit 5 Parametern beschrieben werden kann. Diese sind: das Verhältnis von Froude- und Reynolds-Zahl des Dampfes, die Auftriebszahl, das Verhältnis der Viskositäten von Dampf und Flüssigkeit, die Prandtl-Zahl der Flüssigkeit und die Unterkühlungs-Zahl. Eine numerische Lösung des sich ergebenden Satzes von Gleichungen zeigt merkliche Veränderungen in der Hydrodynamik und beim Wärmetransport, wenn die genannten Parameter variiert werden. Es wurde auch ein Vergleich der Ergebnisse mit Nusselts analytischer Lösung (Wasserhaut-Theorie) durchgeführt mit dem Ergebnis, daß sich nach dieser Theorie bei hohen Drücken, großen Prandtl-Zahlen und bei großem Verhältnis von Froude- zur Reynolds-Zahl die Kondensationslänge und die Filmdicke zu klein und der Stoff- und Wärmetransport zu groß ergibt. Bei kleinen Prandtl-Zahlen zeigen sich gravierende Unterschiede zwischen der analytischen und der numerischen Lösung sowohl für den Wärmetransport als auch für die Hydrodynamik. Diese Unterschiede sind eine Folge der Vernachlässigung der Trägheitsglieder in den Bewegungsgleichungen von Flüssigkeit und Dampf bei der analytischen Lösung und ihrer Berücksichtigung im hier vorgestellten Modell.

ЛАМИНАРНАЯ ПЛЁНОЧНАЯ КОНДЕНСАЦИЯ ЧИСТОГО НАСЫЩЕННОГО ПАРА В ВЕРТИКАЛЬНОЙ ТРУБЕ ПРИ ВЫНУЖДЕННОМ ТЕЧЕНИИ

Аннотация — Проведено аналитическое исследование стационарной ламинарной пленочной конденсации насыщенного пара при вынужденном течении в вертикальной трубе в случае полностью развитого профиля скорости пара на входе в трубу и постоянной температуры стенки трубы.

Уравнения и граничные условия, описывающие процесс конденсации, исследовались подробно с целью определения соответствующих параметров задачи. Для широкого диапазона условий, представляющих практический интерес, найдено, что процесс конденсации описывается пятью параметрами: отношением числа Фруда к числу Рейнольдса для пара, числом плавучести, отношением вязкости пара к вязкости жидкости, числом Прандтля для жидкости и числом недогрева.

Численное решение полученной системы уравнений показывает, что при изменении этих параметров наблюдаются значительные различия в гидродинамике и теплообмене. Также проведено сравнение результатов с аналитическим решением Нуссельта для постоянного межфазового сдвига и найдено, что при больших давлениях, высоких значениях числа Прандтля и высоких значениях отношения числа Фруда к числу Рейнольдса, аналитическое решение Нуссельта занижает длину конденсации и толщину плёнки и завышает величину межфазового тепло- и массообмена. При низких значениях числа Рейнольдса наблюдаются значительные расхождения между аналитическими и численными решениями как в результатах по теплообмену, так и по гидродинамике. Эти расхождения являются следствием пренебрежения инерционными членами в уравнениях движения жидкости и пара в аналитической модели и их учёта моделью, представленной в данной работе.